Detection and Control of Individual Nuclear Spins Using a Weakly Coupled Electron Spin

T. H. Taminiau, J. J. T. Wagenaar, T. van der Sar, F. Jelezko, V. V. Dobrovitski, and R. Hanson

Detection and control of individual nuclear spins using a weakly coupled electron spin

T. H. Taminiau[1], J. J. T. Wagenaar[1], T. van der Sar[1],
F. Jelezko[2], V. V. Dobrovitski[3], and R. Hanson[1]
[1]Kavli Institute of Nanoscience, Delft University of Technology,
PO Box 5046, 2600 GA Delft, The Netherlands.
[2]Institut für Quantenoptik, Universität Ulm, 89081 Ulm, Germany.
[3]Ames Laboratory and Iowa State University, Ames, Iowa 50011, USA.

We experimentally isolate, characterize and coherently control up to six individual nuclear spins that are weakly coupled to an electron spin in diamond. Our method employs multi-pulse sequences on the electron spin that resonantly amplify the interaction with a selected nuclear spin and at the same time dynamically suppress decoherence caused by the rest of the spin bath. We are able to address nuclear spins with interaction strengths that are an order of magnitude smaller than the electron spin dephasing rate. Our results provide a route towards tomography with single-nuclear-spin sensitivity and greatly extend the number of available quantum bits for quantum information processing in diamond.

Detecting the weak magnetic moment of a single nuclear spin presents the ultimate limit of sensitivity in magnetic resonance imaging [1–3]. Furthermore, nuclear spins may play a key role as qubits with long coherence times in quantum information technologies [4]. Addressing and controlling single nuclear spins is challenging because the spins are generally embedded in a noisy environment, such as a surrounding bath of nuclear spins.

The electron spin of a nitrogen-vacancy (NV) center is a powerful probe of its local magnetic environment [2, 3, 5–11]. If a single or a few nuclear spins are located particularly close to an NV center, the hyperfine interaction can well exceed the electron spin dephasing rate $\sim 1/T_2^*$ [12]. Such strongly coupled nuclear spins are readily distinguished from the rest of the spin bath [13, 14] and can be selectively addressed and controlled [15–22]. However, typically the nuclear spin of interest is embedded in a bath of fluctuating nuclear spins. As a result, the coupling of this single nuclear spin to the NV center is weak compared to the rate of electron spin dephasing induced by the spin bath. For both magnetometry and quantum information purposes it would be greatly beneficial to be able to individually resolve and address such weakly coupled nuclear spins.

In this Letter, we isolate, characterize and selectively control up to six weakly coupled ^{13}C nuclear spins that are embedded in the spin bath surrounding an NV center. The weak signal of a specific nuclear spin is amplified by precisely tuning a multi-pulse control sequence on the NV electron spin into resonance with the electron-nuclear spin dynamics [23]. At the same time this sequence dynamically decouples the electron spin from all other nuclear spins [24–26]. With this technique, we are able to resolve and coherently control nuclear spins with couplings that are an order of magnitude smaller than the dephasing rate of the NV center. Our results can enable tomography with single nuclear spin sensitivity and have the potential to greatly extend the number of solid-state spin qubits available for quantum information processing.

Our method to isolate a weakly coupled nuclear spin from a background of other nuclear spins is based on the distinct conditional precession of each nuclear spin due to its particular hyperfine interaction with the NV electron spin ($S = 1$), Fig. 1(a). For the electron in $m_s = 0$, all nuclear spins precess with the Larmor frequency ω_L around an axis parallel to the applied magnetic field $\mathbf{B}_0$. For $m_s = -1$, each nuclear spin precesses around a
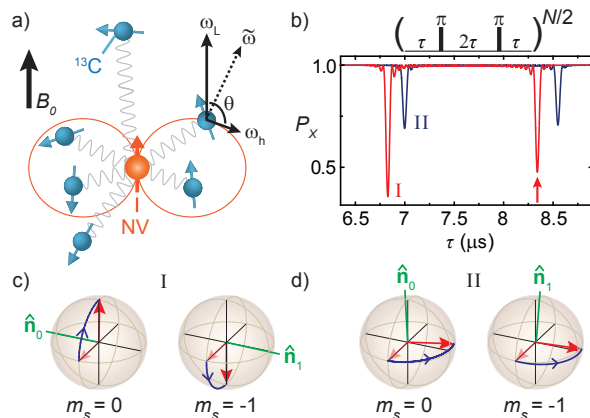

FIG. 1: Concept of isolating and controlling weakly coupled spins. (a) Surrounding ^{13}C nuclear spins precess about axes that depend on the NV electron spin state. For $m_s = 0$, all ^{13}C spins precess about $\boldsymbol{\omega}_L$ set by the applied magnetic field $\mathbf{B}_0$. For $m_s = -1$, each spin precesses about a distinct axes $\tilde{\boldsymbol{\omega}}$ due to the hyperfine interaction $\boldsymbol{\omega}_h$. (b) Calculated probability P_x to preserve the initial electron spin state after a decoupling sequence with $N = 32$, for two ^{13}C spins with $\theta = \pi/4.5$, Nucleus I: $\omega_h = 2\pi \cdot 40$ kHz, Nucleus II: $\omega_h = 2\pi \cdot 20$ kHz, B_0=293 G. Each spin can be selectively addressed by tuning the inter-pulse delay 2τ into resonance with its dynamics. (c,d) Bloch spheres showing the nuclear spin dynamics for τ resonant with nucleus I (arrow). (c) For nucleus I, the net result is a rotation around anti-parallel axes ($\hat{\mathbf{n}}_0$ and $\hat{\mathbf{n}}_1$) for the two electron states, resulting in entanglement. (d) Nucleus II is decoupled: its rotation is independent of the electron state.

distinct axis $\tilde{\boldsymbol{\omega}} = \boldsymbol{\omega}_L + \boldsymbol{\omega}_h$. The hyperfine interaction $\boldsymbol{\omega}_h$ depends on the position of that particular nuclear spin relative to the NV center.

We can probe this conditional interaction by preparing the electron spin in a superposition, $|x\rangle = (|m_s = 0\rangle + |m_s = -1\rangle)/\sqrt{2}$, and applying a dynamical decoupling sequence consisting of N sequential π-pulses. Consider the basic decoupling unit on the electron spin $\tau - \pi - 2\tau - \pi - \tau$, in which τ is a free evolution time (Fig. 1(b)). The net result of this unit is a rotation of the nuclear spin by an angle ϕ around an axis $\hat{\mathbf{n}}_i$ that depends on the initial state of the electron spin: $\hat{\mathbf{n}}_0$ for initial state $m_s = 0$ and $\hat{\mathbf{n}}_1$ for initial state $m_s = -1$ [23, 27].

If $\hat{\mathbf{n}}_0$ and $\hat{\mathbf{n}}_1$ are not parallel, the resulting conditional rotation of the nuclear spin generally entangles the electron and nuclear spins. As a result, for an unpolarized nuclear spin state, the final electron spin state is a statistical mixture of $|x\rangle$ and $|-x\rangle = (|m_s{=}0\rangle - |m_s{=}{-}1\rangle)/\sqrt{2}$. The probability that the initial state $|x\rangle$ is preserved is given by

$$P_x = (M + 1)/2, \tag{1}$$

with for a single nuclear spin:

$$M = 1 - (1 - \hat{\mathbf{n}}_0 \cdot \hat{\mathbf{n}}_1)\sin^2\frac{N\phi}{2}. \tag{2}$$

For multiple nuclear spins that do not mutually interact, M is given by the product of all the individual values M_j for each individual spin j. Analytical expressions for ϕ and for the angle between $\hat{\mathbf{n}}_0$ and $\hat{\mathbf{n}}_1$ as a function of the hyperfine interaction $\boldsymbol{\omega}_h$ and the inter-pulse delay τ are given in the supplemental material [27].

As an example, Fig. 1(b) shows calculated results for two ^{13}C spins with different hyperfine interactions. For most values of τ the NV spin is effectively decoupled from both nuclear spins and its initial state is conserved ($P_x \approx 1$). For specific values of τ, the sequence is precisely resonant for one of the ^{13}C spins and a sharp dip in the signal is observed. Figures 1(c, d) illustrate the evolution of the nuclear spins at the resonance condition for nuclear spin I. At this value of τ, the net rotation axes $\hat{\mathbf{n}}_0$ and $\hat{\mathbf{n}}_1$ for nuclear spin I are approximately *anti*-parallel and the resulting conditional rotation entangles nuclear spin I with the electron spin ($P_x \approx 1/2$). In contrast, at the same value of τ, $\hat{\mathbf{n}}_0$ and $\hat{\mathbf{n}}_1$ are nearly parallel for nuclear spin II and the resulting unconditional rotation leaves the electron spin unaffected. These resonances appear periodically as a function of τ.

More insight into the periodicity and depth of the resonances can be gained by considering the case of large magnetic field, $\omega_L \gg \omega_h$. In this case the positions of the resonances are given by [27]:

$$\tau_k = \frac{(2k - 1)\pi}{2\omega_L + A}, \tag{3}$$

where $k = 1, 2, 3..$ is the order of the resonance, and A is the parallel component of the hyperfine interaction $A = \omega_h \cos\theta$. Equation 3 shows that the position is a linear function of k. The amplitude of the resonances is governed by the rotation angle ϕ, which is of order B/ω_L, with $B = \omega_h \sin\theta$ the perpendicular component of the hyperfine coupling. Although ϕ is small, the total angle is amplified by the large number of pulses N, enabling the detection with maximum contrast even of weakly coupled spins. In this way a single nuclear spin can be isolated from a bath of spins by a judicious choice of the inter-pulse delay 2τ and the number of pulses N.

We experimentally demonstrate our method using an NV center in a type IIa diamond with a natural abundance of ^{13}C nuclear spins (1.1%). All experiments are performed at room temperature with an applied magnetic field along the NV symmetry axis. The NV electron spin is prepared in $m_s = 0$ by illumination with a 532 nm laser and read out through its spin-dependent fluorescence. The experimental setup is described in detail in Ref. 23.

We choose an NV center that shows no nearby strongly coupled ^{13}C spins in the electron spin resonance (ESR) spectrum and Ramsey measurements. The hyperfine coupling to the NV spin of all individual ^{13}C spins is thus weak compared to $1/T_2^*$: all individual nuclear spins are hidden in the spin bath.

The experimental signal for a decoupling sequence with 32 π-pulses is shown in Fig. 2(a). We observe sharp dips and broader collapses in an approximately exponentially decaying signal (see Fig. 2(b) for a magnification). The broader collapses correspond to the overlapping signals of multiple nuclear spins in the spin bath, whose product tends to yield $P_x \approx 0.5$ [28, 29]. The sharp dips are signatures of the resonances of individual ^{13}C spins. These appear primarily for large τ because the separation between resonances of different spins increases with the resonance order k (see Eq. 3). We exploit the linear dependence in Eq. 3 to identify five distinct ^{13}C spins (Fig. 2(c)). The resonances assigned to these spins are indicated in Fig. 2(b).

With a fit based on Eq. 2 we are able to determine both the magnitude ω_h and the angle θ of the hyperfine coupling from the experimentally observed resonances in Fig. 2(b) for each of the five spins. These fits take the overall signal decay due to relaxation to $m_s = +1$ and dephasing of the electron state into account [27]. Although nuclear spin 6 can not be clearly resolved from the spin bath with a sequence of 32 pulses (Fig. 2(b)), we can further increase the sensitivity by applying more pulses. For $N = 96$ the signal for spin 6 is well-isolated from the spin bath (Fig. 2(d)), enabling the characterization of the hyperfine interaction.

The obtained values for the hyperfine interaction strength ω_h and angle θ for the six nuclear spins are listed in Table 1. These values should be compared to the min-
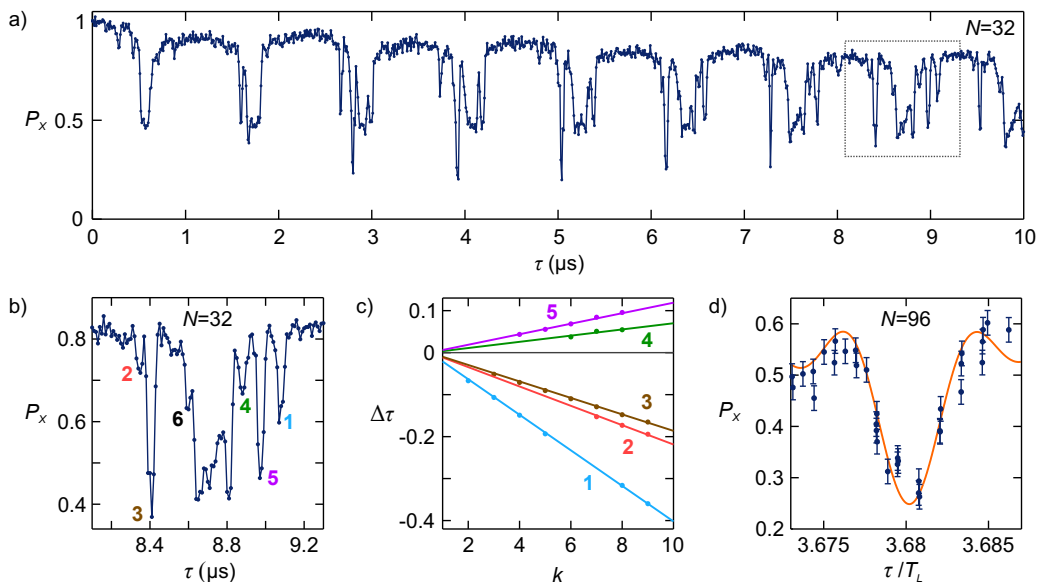
FIG. 2: Resolving individual weakly coupled ^{13}C nuclear spins. (a) P_x as function of τ for a decoupling sequence with $N = 32$ and a magnetic field $B_0 = 401$ G. The sharp resonances in the echo signal correspond to the coherent interaction with individual ^{13}C atoms. (b) Magnification of the section marked in (a) indicating resonances associated with six nuclear spins. (c) Positions τ_k of resonances with order k observed in (a) relative to the Larmor period $T_L = 2\pi/\omega_L$, $\Delta\tau = \tau_k/T_L - (2k-1)/4$. The five sets of equally-spaced resonances correspond to the spins numbered in (b). Lines are fits to Eq. 3. (d) Close up for nuclear spin 6 ($\tau \approx 8.57...8.59$ μs) with $N = 96$. Line: fit based on equation 2. Errors are ± 1 standard deviation (s.d.).

Spin	$\omega_h/2\pi$ (kHz)	θ (degrees)
1	83.8(6)	21(1)
2	47(2)	30(5)
3	55(2)	54(2)
4	19(1)	133(3)
5	33(1)	132(1)
6	25.1(7)	51(2)

TABLE I: Hyperfine coupling strength ω_h and angle θ for the six nuclear spins identified in Fig. 2. For each nuclear spin these values were obtained by individually fitting a single well-isolated resonance based on equation 2. Uncertainties are 2 s.d.
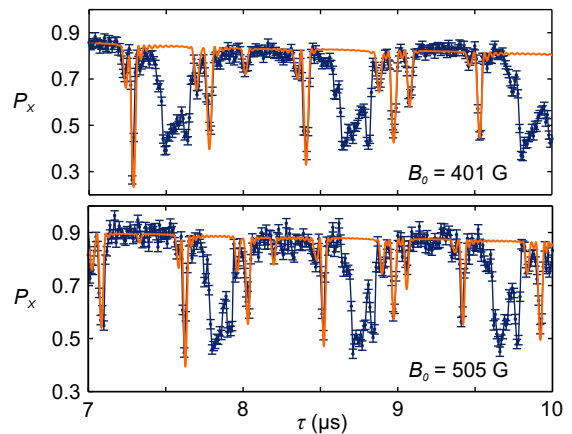

FIG. 3: Comparison of the measured signal with the prediction based on the parameters in Table 1 (orange line). We observe good agreement for the positions and amplitudes of multiple resonances for magnetic fields of both $B_0 = 401$ G and $B_0 = 505$ G. Error bars are ± 1 s.d.

imal coupling that can be resolved in an ESR measurement, which is given by the ESR line width. We find that our method detects hyperfine strengths as small as ~ 20 kHz, about an order of magnitude smaller than the measured line width of $\sqrt{2}/(\pi T_2^*) = 161(1)$ kHz. Furthermore, we resolve differences in hyperfine strength down to ~ 10 kHz.

Assuming that the interaction is purely dipole-dipole, the values in Table 1 correspond to distances to the NV center between 0.6 and 1.2 nm. The fact that we can distinguish multiple weakly coupled spins beyond those that are coupled strongest to the NV demonstrates that our method can be used to create tomographic images of the spin environment at the single nuclear spin level.

We validate our approach by calculating the signal expected from the values in Table 1, and comparing the re-

sult with independent measurements over a broad range of free evolution times at two different magnetic fields (Fig. 3). We find excellent agreement for both the positions and amplitudes of the resonances, confirming the accuracy of the theoretical model and the determined parameters.

Finally, we demonstrate that we can coherently rotate a weakly coupled nuclear spin over a desired angle by tuning the number of pulses N. Figure 4(a) plots the
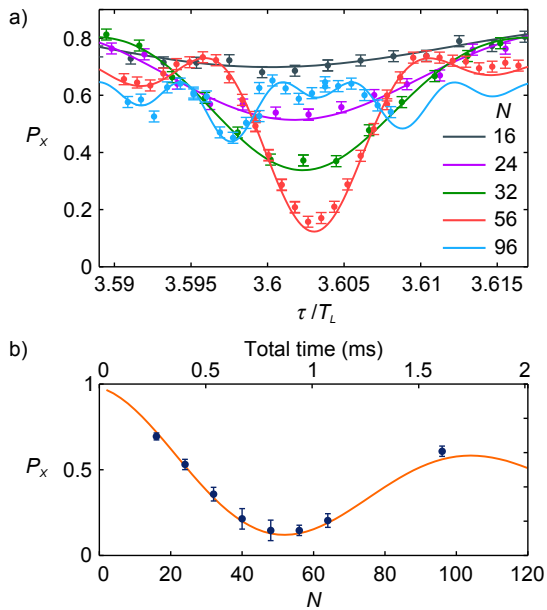
FIG. 4: Coherent conditional rotations of weakly-coupled nuclear spin 3. (a) P_x with different numbers of pulses N for the resonance centered at $\tau \approx 8.4$ μs. Lines: calculations based on the values in Table 1. Error bars: ± 1 s.d. (b) P_x at resonance as function of N. A fit using the values in Table 1 (line) yields a decay constant for the oscillation of 1.8(3) ms (supplementary information). The top horizontal axis shows the total length of the gate. Uncertainties are 2 s.d.

signal for a selected resonance ($k = 8$) of spin 3 for different number of pulses N. The depth of the resonance first increases with N until the maximum contrast is obtained for $N = \pi/\phi \approx 56$. For more pulses the depth decreases again. In Fig. 4(b) we plot the signal at the center of the resonance as a function of N.

The oscillation observed in Fig. 4(b) demonstrates the coherent conditional rotation of a single weakly coupled ^{13}C spin. For $N = 28$ the signal reaches ~ 0.5. Here, the nuclear spin has rotated over an angle $N\phi/2 \approx \pi/2$, in a direction which is conditioned by the electron spin state (similar to the case illustrated in Fig. 1(c)). This sequence corresponds to a maximally entangling operation, equivalent to the quantum controlled-NOT gate up to single-qubit rotations. For $N = 56$, the nuclear spin has rotated over an angle $N\phi/2 \approx \pi$. Here, the two conditional rotations lead to the same final nuclear spin state up to a 2π phase difference. This phase difference transfers to the electron spin, yielding the pure state $|-x\rangle$ and signal $P_x \approx 0$.

Unconditional coherent rotations of the nuclear spin can be implemented by using different values for τ (see e.g. Fig. 1(d)) [23]. A combination of conditional and unconditional operations can be used to initialize the nuclear spin by swapping its state with the electron [15] or for reading out the nuclear spin state in a single-shot by mapping it onto the electron spin [18, 21, 22]. Our re-

sults thus indicate the possibility of using weakly coupled nuclear spins as fully controllable qubits.

The oscillation in Fig. 4(b) is damped on a timescale of a few ms. This timescale is consistent with the coherence time being limited by the longitudinal relaxation of the electron spin at room temperature (T_1 process) [30]. At cryogenic temperatures this relaxation time exceeds seconds [30], lifting this limitation and thus potentially allowing for the implementation of multiple high-precision quantum gates on weakly coupled ^{13}C nuclei.

In conclusion, we have isolated, characterized and coherently controlled individual weakly coupled nuclear spins embedded in a spin bath. Because we address spins beyond the few nearest to the NV center, our method can enable the tomography of ensembles of spins in diamond and, potentially, in external samples [31]. In addition, the method enables coherent gates between the electron spin and weakly-coupled nuclear spins and could be extended to other electron-nuclear systems such as phosphorous donors in silicon [32, 33]. Our results thus indicate a clear pathway for using weakly coupled nuclear spins as a qubit register controlled by the electron, thereby eliminating the need for strong coupling and greatly extending the possible number of qubits within a local register.

[1] C. L. Degen *et al.*, Proc. Nat. Acad. Sci. **106**, 1313 (2009).
[2] J. M. Taylor *et al.*, Nature Phys. **4**, 810 (2008).
[3] C. L. Degen, Appl. Phys. Lett. **92**, 243111 (2008).
[4] T. D. Ladd *et al.*, Nature **464**, 45 (2010).
[5] J. R. Maze *et al.*, Nature **455**, 644 (2008).
[6] G. Balasubramanian *et al.*, Nature **455**, 648 (2008).
[7] G. de Lange *et al.*, Phys. Rev. Lett. **106**, 080802 (2011).
[8] N. Zhao *et al.*, Nature Nanotech. **6**, 242 (2011).
[9] L. Rondin *et al.*, Appl. Phys. Lett. **100**, 153118 (2012).
[10] S. Kolkowitz *et al.*, Science **335**, 1603 (2012).
[11] L. T. Hall *et al.*, Phys. Rev. B **82**, 045208 (2010).
[12] L. Childress *et al.*, Science **314**, 281 (2006).
[13] B. Smeltzer *et al.*, New J. Phys. **13**, 025021(2011).

[14] A. Dréau *et al.*, Phys. Rev. B **85**, 134107 (2012).
[15] M. V. G. Dutt *et al.*, Science **316**, 1312 (2007).
[16] P. Neumann *et al.*, Science **320**, 1326 (2008).
[17] B. Smeltzer *et al.*, Phys. Rev. A **80**, 050302 (2009).
[18] P. Neumann *et al.*, Science **329**, 542 (2010).
[19] M. Steiner *et al.*, Phys. Rev. B **81**, 035205 (2010).
[20] G. D. Fuchs *et al.*, Nature Phys. **7**, 789 (2011).
[21] L. Jiang *et al.*, Science **326**, 267 (2009).
[22] L. Robledo *et al.*, Nature **477**, 574 (2011).
[23] T. van der Sar *et al.*, Nature **484**, 82 (2012).
[24] G. de Lange *et al.*, Science **330**, 60 (2010).
[25] C. A. Ryan *et al.*, Phys. Rev. Lett. **105**, 200402 (2010).
[26] B. Naydenov *et al.*, Phys. Rev. B **83**, 081201 (2011).
[27] See Supplemental Material for derivations of the equations used and a description of the fitting including relaxation and dephasing.
[28] E. van Oort *et al.*, Chem. Phys. **143**, 131 (1990).
[29] N. Zhao *et al.*, Phys. Rev. B **85**, 115303 (2012).
[30] A. Jarmola *et al.*, arXiv:1112.5936v2 (2012).
[31] J. -M. Cai *et al.*, arXiv:1112.5502v1 (2011).
[32] J. J. L. Morton *et al.*, Nature **455**, 1085 (2008).
[33] A. Morello *et al.*, Nature **467**, 687 (2010).
[34] S. Kolkowitz *et al.*, arXiv:1204.5483v1 (2012).
[35] N. Zhao *et al.*, arXiv:1204.6513v1 (2012).